J. Fluid Mech. (1982), *vol.* 117, *pp.* 315–341
Printed in Great Britain

Internal-wave interactions in the induced-diffusion approximation

By JAMES D. MEISS†
Department of Physics, University of California, Berkeley
AND KENNETH M. WATSON‡
Center for Studies of Nonlinear Dynamics, La Jolla Institute, P.O. Box 1434, La Jolla, CA 92038

(Received 6 August 1980 and in revised form 4 August 1981)

Dynamical equations for the interaction of high-wavenumber, high-frequency internal waves with a prescribed, linear, large-scale internal-wave field are obtained from the Boussinesq–Euler equations. The relationship of these 'induced-diffusion' interactions to the Taylor–Goldstein equation is discussed. Exact equations are derived in the induced-diffusion limit of McComas & Bretherton (1977) for the evolution of the first and second moments of the small-scale flow when the large-scale flow is assumed random. Estimates of corrections to the induced-diffusion approximation for the Garrett–Munk internal-wave model indicate the domain of applicability of these equations. Computations of the autocorrelation function and action transport in wavenumber and physical space are presented. Severe limitations are found on the applicability of two-time perturbation theory and the resonant-interaction approximation. The high transfer rates found by McComas & Bretherton in the induced-diffusion regime are reduced significantly in the present calculations.

1. Introduction

Weakly nonlinear interactions among waves occur in a variety of physical systems. To describe these processes for macroscopic media, such as those encountered in plasma physics and geophysics, the radiative-transport equation is frequently used (Hasselmann 1966, 1967; Davidson 1972). Unfortunately, the accuracy of such approximation methods has been difficult to assess. In this paper we shall study a specific application which is of sufficient simplicity for a detailed analysis.

The physical process that we shall study is the interaction of small-scale internal waves with a much larger-scale internal-wave field. Our dynamical description is based on a time-dependent form of the Taylor–Goldstein equation (Bretherton 1966; Booker & Bretherton 1967; Leblond & Mysak 1979) that has been used to study critical-layer phenomena. For our use of this equation the vertically sheared, horizontal flow results from the large-scale, near-inertial-frequency, portion of the internal-wave spectrum.

For internal waves in the ocean, the observational data suggest a universal

† Present address: Institute for Fusion Studies, University of Texas, Austin, Texas
‡ Present Address: Marine Physical Laboratory of the Scripps Institution of Oceanography, University of California, San Diego, La Jolla, CA 92093

'equilibrium' velocity spectrum (Garrett & Munk 1979, hereinafter referred to as GM). McComas & Bretherton (1977, hereinafter referred to as MB) have applied the Hasselmann transport equation to a detailed study of transfer processes within the internal-wave spectrum. Other discussions of internal wave transport have been given by Olbers (1976), who also used the Hasselmann radiative-transfer equation, and by Meiss, Pomphrey and Watson (Meiss, Pomphrey & Watson 1979, hereinafter referred to as MPW; Pomphrey, Meiss & Watson 1980, hereinafter referred to as PMW), who based their discussion on the Langevin and Fokker–Planck equations. (A similar study of Rossby waves has been given by Holloway & Hendershott (1977).)

The analyses of MB, Olbers and PMW all use some form of 'weak-nonlinearity' perturbation approximation. In particular, the wave–wave couplings are restricted to triad, or three-wave interactions† and a separation of 'fast' and 'slow' time scales is assumed. A radiative-transfer equation for the action density $F(\mathbf{k})$ in the wavenumber space is obtained. This has the form

$$\frac{\partial F(\mathbf{k})}{\partial t} = I(\mathbf{k}) - 2\nu_{\mathrm{P}}(\mathbf{k})\, F(\mathbf{k}). \tag{1.1}$$

Here $I(\mathbf{k}) \geqslant 0$ represents the flow of action into wavenumbers near $\mathbf{k}$. This is an integral operator which is quadratic in F. It was demonstrated in PMW that ν_{P} is the 'Langevin rate constant', which describes the decorrelation rate of the Fourier amplitudes of the internal-wave field. A 'Boltzmann rate' was introduced in PMW as

$$2\nu_{\mathrm{B}}(\mathbf{k}) \equiv [I - 2\nu_{\mathrm{P}} F]/F. \tag{1.2}$$

It was shown in PMW that $2\nu_{\mathrm{P}}$ represents the rates calculated by McComas (1977) in his 'bump experiments'. The quantity $2\nu_{\mathrm{B}}$ describes the net rate of action transport.

The calculations of MB using (1.1) indicated that the empirical GM spectrum represents – to an approximation – a steady-state solution of the radiative-transfer equation, except for specific wavenumber domains where sources and/or sinks of energy appear to occur. Unfortunately, the computed transfer rates indicate that the 'weak-nonlinearity' assumption fails drastically for the higher-vertical-wavenumber portion of the spectrum (see figure 1 of PMW or Holloway (1980)). The physical significance of the calculated transfer rates has consequently been unclear.

McComas & Bretherton identify three limiting forms of triad interactions as being of particular significance for the transport equation (1.1). It is the mechanism called *induced diffusion* by MB with which we shall be concerned in this paper. The induced-diffusion triads consist of two waves with high wavenumber and high frequency interacting with a third wave of much smaller wavenumber and frequency. In the high-vertical-wavenumber, high-frequency regime the induced-diffusion mechanism gives the principal contribution to the right-hand side of (1.1) and is also responsible for the high transfer rates that have cast doubt on the applicability of (1.1).

The calculations presented in this paper are based on the Taylor–Goldstein equation. An ensemble average is performed over realizations of the large-scale flow, which is assumed to consist of linear internal waves with nearly inertial frequencies. Evolution equations for the first three moments of the Fourier-amplitude coefficients of the small-

† Pomphrey (1981) has shown that for the constant-N model of MB and Olbers the restriction to triad interactions is exact. For the GM scaling used by PMW corrections are not thought to be significant.

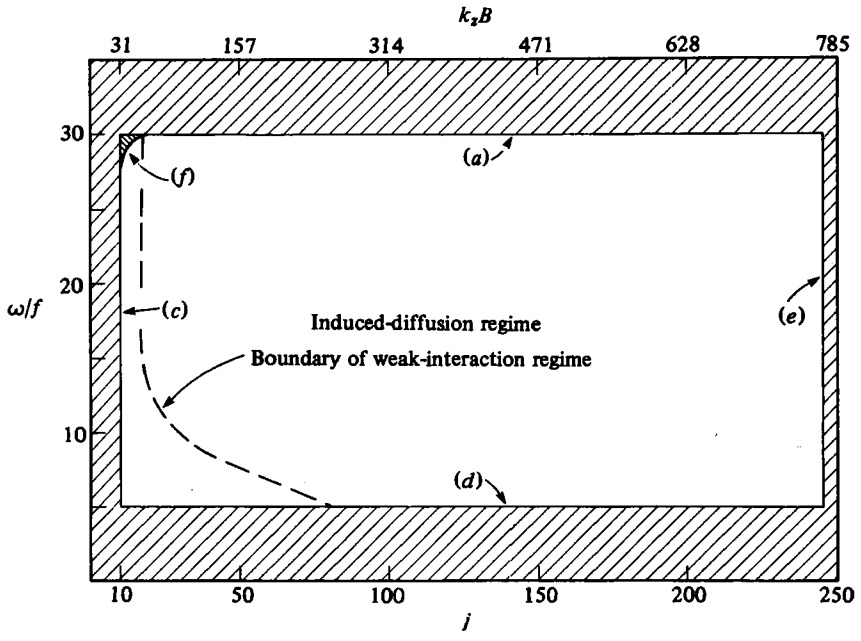

FIGURE 1. The induced-diffusion approximation and the calculations of this paper are valid within the rectangle. Letters label conditions (2.1) that fail at the boundaries.

scale flow are derived. The first moment describes the decay of the autocorrelation function. It also gives the relaxation rate ν_P when the spectrum is perturbed from 'equilibrium' (PMW; McComas 1977). The equation for the second moment describes the evolution of action density in co-ordinate and wavenumber space – a modified form of (1.1). The third moment corresponds to the bispectrum.

The first two moments are deduced from the induced-diffusion limit of the Taylor–Goldstein equation without approximation. Corrections to the induced-diffusion limit are obtained by perturbation theory.

The domain in frequency–vertical-wavenumber space for which our calculations are considered to be valid is shown as the unshaded rectangle in figure 1. Here f is the inertial frequency (a latitude of 30° has been assumed), k_z is the vertical wavenumber and $B = 1{\cdot}2$ km is the GM scale length. We have related k_z to the discrete eigenmode number j with the WKB relation

$$k_z B \simeq \pi j \quad (j = 1, 2, \ldots). \tag{1.3}$$

The left-hand boundary at $j = 10$ is suggested by figure 7 of PMW; for $j \geqslant 10$ the induced diffusion limit was found to account for ν_P to within the numerical accuracy of the calculation (limited by truncation at high mode numbers). The lower limit at $\omega/f = 5$ is suggested by figure 4 of PMW. The upper limit at $\omega/f \simeq 30$ has been set in part to permit the use of a simple WKB approximation (see the discussion of this in MB and PMB) and in part because of observations by Pinkel (1975) and also a study by Yau (1981) which indicate that at higher frequencies effects due to the thermocline and the mixed layer need be accounted for in (1.1). The right-hand boundary at $j \simeq 250$ represents the limit of validity anticipated for the Taylor–Goldstein equation.

In the following sections of this paper we shall develop the induced diffusion theory

for the 'allowed region' in figure 1 – that is, the area within the unshaded rectangle. The value of ν_P obtained in this region will appear to have a relative error of less than 10 % (with the possible exception of the boundary at $j \simeq 250$. A comparable validity for (1.1) is inferred. The very high transfer rates found by MB and PMW in the induced diffusion regime are not found in our present calculations. Indeed, ν_P is no longer found to be significantly greater than the linear-wave angular frequency. Also, the resonant-triad approximation, which results from the use of two-time perturbation theory, is found to be grossly in error in the region of figure 1 that is to the right of the dashed line labelled 'boundary of weak-interaction regime' (cf. Holloway (1979), who suggests a technique to model non-resonant interactions).

The calculated Langevin rates for the domains $j < 10$ or $\omega/f < 5$ do not violate the 'weak-interaction' postulate,† so the Hasselmann theory for (1.1) may be hoped to be valid in these regions.

The elastic-scattering mechanism of MB represents a correction to induced diffusion in the allowed region of figure 1. Watson (1981) shows that the elastic-scattering Langevin constant does not violate the 'weak-interaction' assumption and that this is much smaller than that due to induced diffusion in the allowed region.

Müller (1976) has considered the interaction of a small-scale internal wave field with quasi-geostrophic flows, treated as static. A WKB approximation was used by Müller. His calculations are not directly comparable to those presented here because of the time variation of the large-scale wave field.

2. Induced-diffusion approximation

2.1. *Dynamics*

To develop the induced-diffusion hydrodynamic model we choose a rectangular coordinate system with the (x, y)-plane coincident with the ocean surface and the z-axis directed upward. We make the Boussinesq approximation‡ (Phillips 1977) and assume incompressible flow. In the absence of waves, the fluid is stably stratified with density $\rho = \bar{\rho}(z)$.

For the induced-diffusion approximation (IDA) the flow field is assumed to consist of large- and small-scale components. The small-scale flow is due to internal waves characterized by horizontal and vertical wavenumbers k_h and k_z, and the horizontal and vertical components of the fluid velocity $\mathbf{u}$ and w respectively. The large-scale flow is characterized by wavenumbers l_h and l_z, and a horizontal fluid velocity $\mathbf{U}$. The vertical velocity of the large-scale flow is neglected. Angular frequencies for the small- and large-scale flows are ω_k and ω_l.

The observed properties of the internal wave field in the ocean (Garrett & Munk 1979) suggest that the approximations

$$k_h \ll k_z, \quad l_h \ll l_z \tag{2.1a}$$

are reasonable. Following MB, the induced-diffusion class of triads have the properties

$$k_h \gg l_h, \quad k_z \gg l_z, \quad \omega_k \gg \omega_l. \tag{2.1b, c, d}$$

† This is marginal in the lower right-hand corner in figure 1.

‡ We recall that the Boussinesq approximation was made by PMW only in the final stage of numerical evaluation.

The linear Taylor–Goldstein equation is valid, or

$$\epsilon \equiv \langle (\partial \xi_z/\partial z)^2 \rangle \ll 1, \quad \omega_l \simeq f. \tag{2.1e,f}$$

Here f, the inertial frequency, enters through the Coriolis term in Euler's equations. The expression $\langle\ \rangle$ represents an average over the GM spectrum and the vertical displacement ξ_z is defined by (2.3) below.

It is consistent with the IDA to assume that $\mathbf{U}(r,t)$ is a prescribed velocity field that results from a superposition of linear internal waves. Because of the conditions (2.1), the horizontal gradients of U may be neglected. It is straightforward to obtain, from the Euler equations, the two coupled equations

$$D(\nabla^2 w) + \nabla^2 \Omega^2 \xi_z = \frac{\partial^2 \mathbf{U}}{\partial z^2} . \nabla_{\mathrm{h}} w + \frac{\partial}{\partial z}\left(\frac{\partial \mathbf{U}}{\partial z} . \mathbf{f} \times \nabla_{\mathrm{h}} \xi_z\right), \tag{2.2}$$

$$w = D\xi_z. \tag{2.3}$$

Here we have defined

$$\nabla_{\mathrm{h}} = \nabla - \hat{\mathbf{z}} \frac{\partial}{\partial z}, \quad D = \frac{\partial}{\partial t} + \mathbf{U} . \nabla_{\mathrm{h}}, \quad \mathbf{f} = f\hat{\mathbf{z}}, \tag{2.4}$$

and introduced the 'frequency operator'

$$\Omega = \left[\nabla^{-2}\left(f^2 \frac{\partial^2}{\partial z^2} + N^2 \nabla_{\mathrm{h}}^2\right)\right]^{\frac{1}{2}}, \tag{2.5}$$

where N is the Brunt–Väisälä frequency. If the inertial frequency f were zero, (2.2) and (2.3) would reduce to the time-dependent form of the Taylor–Goldstein equation (Bretherton 1966). On the other hand, if both terms on the right-hand side of (2.2) were neglected, we would obtain equations equivalent to the IDA of McComas & Bretherton. These two terms represent the leading corrections to the IDA and will be used to estimate the accuracy of this approximation.

If the vertical component of velocity for the large-scale flow were taken into account, we would replace N^2 in (2.5) by

$$N_{\mathrm{v}}^2 \equiv -\frac{g}{\rho_0} \frac{\partial}{\partial z} \bar{\rho}(z - x_3).$$

Here x_3 is the vertical fluid displacement due to the large-scale flow. The perturbation methods described in § 3 have been used to calculate the contribution from x_3. This was negligibly small, so we are justified in setting $x_3 = 0$ in (2.5).

It is convenient to use a WKB-like approximation for wave propagation in the vertical direction. We assume, following MB, that (2.2–2.3) applies in a rectangular volume of horizontal dimension S_{h} and vertical dimension S_z. Within this volume, N is taken to be a constant.

The system (2.2–2.3) can be reduced to a single equation by defining a complex field variable

$$Z(\mathbf{r}, t) \equiv \Omega^{-1} w - i\xi_z. \tag{2.6}$$

Inversion of this relation yields

$$\xi_z = \tfrac{1}{2} i(Z - Z^*), \quad w = \tfrac{1}{2}\Omega(Z + Z^*). \tag{2.7}$$

The coupled equations (2.4) and (2.5) reduce to a single equation for Z:

$$\frac{\partial}{\partial t} Z + i\Omega Z = S_I + S_N, \tag{2.8}$$

$$S_I = i\mathbf{U}.\nabla_h \xi_z - (\nabla^2\Omega)^{-1}[\mathbf{U}.\nabla_h(\nabla^2 w)], \tag{2.9}$$

$$S_N = (\nabla^2\Omega)^{-1}\left[\frac{\partial^2\mathbf{U}}{\partial z^2}.\nabla_h w + \frac{\partial}{\partial z}\left(\frac{\partial\mathbf{U}}{\partial z}.\mathbf{f}\times\nabla_h\xi_z\right)\right].$$

In the IDA the term S_N would be neglected.

When

$$|S_I| \ll \left|\frac{\partial Z}{\partial t}\right|$$

the 'weak-interaction' condition used to derive (1.1) is valid. Above and to the right of the dashed curve in figure 1 the condition

$$|S_I| \gtrsim \left|\frac{\partial Z}{\partial t}\right|$$

is encountered. This is the domain in which the large-scale velocity U is expected to be comparable to, or exceed, the horizontal phase velocity ω_k/k_h of the small-scale flow. Because of the ensemble-averaging needed to obtain our transport theory, critical layers are 'smeared' in co-ordinate space and are not exhibited explicitly in our calculations. As was observed by Cox & Johnson (1979), the distance that a small-scale wave packet propagates during the time ν_P^{-1} is small compared with B (equation (1.3)) for the waves in the allowed region of figure 1. Thus the explicit time dependence of the large-scale flow must be taken into account in studying induced diffusion.

The Taylor–Goldstein equation describes a small-scale, small-amplitude flow perturbing a large-scale flow. It is linearized in the amplitude of the small flow. The most significant term omitted from Euler's equation appears to be

$$(\mathbf{u}+\hat{\mathbf{z}}w).\nabla(\mathbf{u}+\hat{\mathbf{z}}w), \tag{2.10}$$

which would lead to a correction of order $\epsilon^{\frac{1}{2}}$ (condition (2.1*e*)) with respect to the $D(\nabla^2 w)$ term in (2.2). (The quantity ϵ represents also the inverse Richardson number for the small-scale flow.)

We have indicated in figure 1 by letters corresponding to the various conditions (2.1) the boundaries at which these fail to be valid. The quantity $\epsilon \simeq 0{\cdot}2$ along the boundary at $j = 250$. The term S_N gives a maximum contribution to ν_P of about 10 % along the boundary at $w/f = 5$. In the lower left corner l_z/k_z has a maximum about 0·25 (determined from a resonant-triad condition). The condition (2.1*b*) is very well satisfied everywhere in the allowed region because of the weighting of small horizontal wavenumbers in the GM spectrum.†

With no large-scale flow ($U = 0$), the solutions to (2.8) are linear internal waves

$$Z \propto \exp[i\mathbf{k}.\mathbf{r} - i\omega_{\mathbf{k}}t], \quad \omega_{\mathbf{k}} \equiv \left[\frac{f^2k_z^2 + N^2k_h^2}{k^2}\right]^{\frac{1}{2}} \simeq \left[f^2 + N^2\left\{\frac{k_h}{k_z}\right\}^2\right]^{\frac{1}{2}}. \tag{2.11}$$

We use these solutions as a basis for a Fourier-series representation of the field Z in the volume $S_h^2 S_Z$:

$$Z(\mathbf{r},t) = \sum_{\mathbf{k}}\frac{a_{\mathbf{k}}}{k_h}e^{i\mathbf{k}.\mathbf{r}} = \left(\frac{2}{\rho_0}\right)^{\frac{1}{2}}\sum_{\mathbf{k}}\frac{\mathbf{k}_h}{k_z\omega_{\mathbf{k}}^{\frac{1}{2}}}b_{\mathbf{k}}(t)\,e^{i(\mathbf{k}.\mathbf{r}-\omega_{\mathbf{k}}t)}. \tag{2.12}$$

† This is assured by special properties of the coefficients in the coupled modal equations (Pomphrey 1981).

Here the amplitudes $a_{\mathbf{k}}$ are wave slope variables in the notation of MPW, and the $b_{\mathbf{k}}$ are action-amplitude variables satisfying

$$|b_{\mathbf{k}}|^2 = J_{\mathbf{k}}, \tag{2.13}$$

where $J_{\mathbf{k}}$ is the action per unit volume (see, for example, equation (2.21) of MPW).

The corresponding Fourier expansion for the large-scale velocity is (see equation (2.15) of MPW)

$$\mathbf{U}(\mathbf{r},t) = -\tfrac{1}{2}f\sum_{\mathbf{l}}\frac{l_z}{l_{\mathrm{h}}^2}\{(\hat{\mathbf{l}}_{\mathrm{h}} + i\hat{\mathbf{f}}\times\hat{\mathbf{l}}_{\mathrm{h}})\,a_{\mathbf{l}}(t)\,e^{i\mathbf{l}\cdot\mathbf{x}} + \text{c.c.}\}, \tag{2.14}$$

where the $\hat{}$ indicates a unit vector. The large-scale amplitudes evolve in time according to the linear equations of motion. We define dimensionless amplitudes for the large-scale flow by

$$c_{\mathbf{l}} = \frac{l_z}{Bl_{\mathrm{h}}^2}a_{\mathbf{l}}e^{i(\omega_{\mathbf{l}}t+\phi_{\mathbf{l}})},$$

where B is the GM scale length and the phase is defined by

$$e^{i\phi_{\mathbf{l}}} = i(\hat{\mathbf{l}}_{\mathrm{h}} + i\hat{\mathbf{f}}\times\hat{\mathbf{l}}_{\mathrm{h}})\cdot\hat{\mathbf{m}}_{\mathrm{h}}.$$

We will see that none of our results depend on this phase factor, because we assume that the large-scale flow is homogeneous (see equation (2.19). We therefore 'absorb' the phase into the amplitudes $c_{\mathbf{l}}$ with no loss of generality.

In terms of these variables (2.8) becomes

$$\dot{b}_{\mathbf{k}} = \sum_{\mathbf{m}} A_{\mathbf{k}}^{\mathbf{m}}(t)\,b_{\mathbf{m}}, \tag{2.15a}$$

$$A_{\mathbf{k}}^{\mathbf{m}}(t) \equiv h(\mathbf{k},\mathbf{m})\sum_{\mathbf{l}}[c_{\mathbf{l}}e^{i\Delta_- t}\delta_{\mathbf{k}-\mathbf{m}-\mathbf{l}} - c_{\mathbf{l}}^{*}e^{i\Delta_+ t}\delta_{\mathbf{k}-\mathbf{m}+\mathbf{l}}], \tag{2.15b}$$

$$\Delta_{\pm} \equiv \omega_{\mathbf{k}} - \omega_{\mathbf{m}} \pm \omega_{\mathbf{l}}. \tag{2.15c}$$

There are contributions from both S_I and S_N to the coefficients $h(\mathbf{k},\mathbf{m})$:

$$h(\mathbf{k},\mathbf{m}) = h_I(\mathbf{k},\mathbf{m}) + h_N(\mathbf{k},\mathbf{m}),$$

$$h_I(\mathbf{k},\mathbf{m}) = \tfrac{1}{4}\mathbf{f}[k_z^2\omega_{\mathbf{k}} + m_z^2\omega_{\mathbf{m}}]\frac{B}{k_z m_z}\left\{\frac{k_{\mathrm{h}}m_{\mathrm{h}}}{\omega_{\mathbf{k}}\omega_{\mathbf{m}}}\right\}^{\frac{1}{2}},$$

$$h_N(\mathbf{k},\mathbf{m}) = -\tfrac{1}{4}f(k_{\mathrm{h}}B)\left[\frac{(k_z-m_z)^2}{k_z m_z}\left(\frac{\omega_{\mathbf{m}}}{\omega_{\mathbf{k}}}\right)^{\frac{1}{2}} + \frac{|k_z-m_z|}{m_z}\frac{f}{(\omega_{\mathbf{k}}\omega_{\mathbf{m}})^{\frac{1}{2}}}\right]. \tag{2.16}$$

In obtaining (2.15) and (2.16) we have discarded terms containing $\delta_{\mathbf{k}+\mathbf{m}\pm\mathbf{l}}$ since these are far from resonance. In (2.16) we have set $l_{\mathrm{h}} = 0$ and $k^2 = k_z^2$. The sign of the second term in h_N has been determined from the appropriate triad-resonance condition.

In the IDA the term h_N in (2.16) is neglected and only the symmetric coefficient h_I is used. We will see that if $h(\mathbf{k},\mathbf{m}) = h(\mathbf{m},\mathbf{k})$ the total action is conserved by the transport system.

In addition to the IDA we shall also consider the 'IDA limit'. In this limit the ratio l_z/k_z is considered to be sufficiently small that only the lowest-order terms in this quantity are kept in h_I and $\Delta_{\pm}$.

For the IDA-limit solutions of the following sections, the most important property of the coupling coefficients is that

$$h_I(\mathbf{K},\mathbf{K}) = \tfrac{1}{2}fK_{\mathrm{h}}B, \tag{2.17}$$

is independent of K_z. Since h_I is symmetric, the corrections to (2.17) arise only at second order:

$$h_I(\mathbf{K}+\tfrac{1}{2}l, \mathbf{K}-\tfrac{1}{2}l) = h_I(\mathbf{K},\mathbf{K})\left[1+\frac{1}{8}\left(\frac{l_z}{K_z}\right)^2+O\left(\frac{l_z}{K_z}\right)^4\right]. \tag{2.18}$$

Because of the very small values expected for l_h by (2.1), $h_I(\mathbf{K},\mathbf{K})$ may be considered a *constant*, independent of $\mathbf{K}$, when solving (2.15). When l_z is determined from the resonant-triad conditions $\Delta_\pm = 0$, the value of the square bracket in (2.18) differs from unity by less than 1 % in the allowed region of figure 1. For the derivation of 'exact' transport coefficients in §§ 3 and 4, the IDA limit is invoked to permit dropping terms of order $(l_z/K_z)^4$ and higher in (2.18). In this limit we can consider $\mathbf{K}$ to be constant and h_I a function of $\mathbf{l}$ only.

2.2. *Statistical description of the large-scale flow*

As discussed in § 1, we shall treat (2.15) as stochastic differential equations with the large-scale flow, assumed to be a Gaussian random field:

$$\left.\begin{aligned} \langle c_{\mathbf{l}}\rangle &= 0,\\ \langle c^*_{\mathbf{l}'}(t+\tau)\, c_{\mathbf{l}}(t)\rangle &= \delta_{\mathbf{l}'-\mathbf{l}}\langle |c_{\mathbf{l}}|^2\rangle C_{\mathbf{l}}(\tau),\\ \langle c_{\mathbf{l}'}(t')\, c_{\mathbf{l}}(t)\rangle &= 0, \end{aligned}\right\} \tag{2.19}$$

and so forth. Here $C_{\mathbf{l}}$ is the correlation function and $\langle |c_{\mathbf{l}}|^2\rangle$ is the power spectrum.

The large-scale wave correlation time is

$$\tau_c \simeq \left|\int_0^\infty dt'\, C_{\mathbf{l}}(t')\right|. \tag{2.20}$$

If the principal mechanism for decorrelation of the large-scale flow is internal-wave–internal-wave interactions, $\tau_c = (\nu_P)^{-1}$. The calculations of ν_P given in PMW indicate that τ_c is much larger than any other characteristic time encountered here, so we are justified in taking $\tau_c^{-1} = 0$ in this paper and will consider the large-scale flow to result from a linear internal-wave field.

The power spectrum of the amplitudes $c_{\mathbf{l}}$ is related to the spectrum Φ of the velocity field (2.14) by†

$$\sum_{\mathbf{l}} \langle |c_{\mathbf{l}}|^2\rangle = \frac{1}{(Bf)^2}\int d^3\mathbf{l}\, \Phi(\mathbf{l}). \tag{2.21}$$

This power spectrum is related to the vertical displacement spectrum Ψ by (see e.g. MPW)

$$\Phi(l_z, \mathbf{l}_h) = 2\left\{\frac{l_z f}{l_h}\right\}^2 \Psi(l_z, \mathbf{l}_h), \tag{2.22}$$

when horizontal isotropy is assumed. We shall use the GM-76 spectrum for our computations. We shall require only the spectrum of vertical wavenumber:

$$\Phi(l_z) = \int d^2\mathbf{l}_h\, \Phi(l_z, \mathbf{l}_h) = 0{\cdot}13\frac{B^3 f^2}{9+(l_z B/n(z)\,\pi)^2}. \tag{2.23}$$

† We shall freely replace discrete Fourier sums by integrals using the equations

$$\sum_{\mathbf{k}} (\Delta k_h)^2 \Delta k_z = \int d^3\mathbf{k},$$

where $\Delta k_h = 2\pi/S_h$ and $\Delta k_z = 2\pi/S_z$.

Here the GM Väisälä profile is used:

$$N(z) = N_0 e^{z/B} \equiv N_0 n(z), \tag{2.24}$$

where $B = 1200$ m is the scale length and $N_0 = 5{\cdot}2 \times 10^{-3}\ \mathrm{s}^{-1}$ is the extrapolated surface value for the Väisälä frequency. We shall also use the value $f = 0{\cdot}014 N_0$, which corresponds to 30° latitude.

With the spectrum (2.23), the mean-square velocity of the flow is

$$\langle U^2 \rangle = \int dl_z \Phi(l_z) = 0{\cdot}44 (Bf)^2 n(z). \tag{2.25}$$

3. Autocorrelation relaxation

3.1. *The Langevin equation*

In this section we shall obtain a relaxation equation for the amplitude of the small-scale flow averaged over realizations of the large-scale flow. In PMW this was postulated to be of the Langevin form†

$$\frac{d}{dt}\langle b_{\mathbf{k}}(t)\rangle = -\nu_{\mathrm{P}}(\mathbf{k})\langle b_{\mathbf{k}}(t)\rangle,$$

where $\langle\ \rangle$ represents the ensemble average (2.19) over the large flow field. We now derive a (modified) Langevin equation by two different methods. The first method considers only the IDA limit and obtains in this limit an exact result. The second method does not take the IDA limit in (2.15), but employs a perturbation expansion due to Van Kampen (1974*a*, *b*). The leading term of the Van Kampen expansion gives the exact result of the IDA limit and higher-order terms give successive corrections to this. Thus, comparison of these two calculations provides an assessment of the accuracy of our evaluation of the Langevin constant ν_{P}.

We begin with the formal solution of (2.15*a*):

$$\langle b_{\mathbf{k}}(t)\rangle = \sum_{\mathbf{m}} U_{\mathbf{k}}^{\mathbf{m}}(t)\, b_{\mathbf{m}}(0),$$

$$U_{\mathbf{k}}^{\mathbf{m}}(t) = \sum_{n=0}^{\infty} \frac{1}{(2n)!}\int_0^t dt_1 \int_0^t dt_2 \dots \int_0^t dt_{2n}\, T(\langle \mathbf{A}(t_1)\,\mathbf{A}(t_2)\dots\mathbf{A}(t_{2n})\rangle)_{\mathbf{k}}^{\mathbf{m}}, \tag{3.1}$$

where $T(\ )$ represents the time-ordered product. Our first task is to simplify the $2n$th moment of $\mathbf{A}$:

$$\gamma_{\mathrm{L}\mathbf{m}_0}^{\mathbf{m}_{2n}}(t_1 \dots t_{2n}) \equiv \sum_{\mathbf{m}_1 \dots \mathbf{m}_{2n-1}} \langle A_{\mathbf{m}_0}^{\mathbf{m}_1}(t_1)\, A_{\mathbf{m}_1}^{\mathbf{m}_2}(t_2) \dots A_{\mathbf{m}_{2n-1}}^{\mathbf{m}_{2n}}(t_{2n})\rangle. \tag{3.2}$$

Here the ts are labelled consistently with the time-ordered product.

Because we have assumed that the $c_{\mathbf{l}}$s are uncorrelated Gaussian variables, we may evaluate (3.2) in terms of the second moments

$$\langle A_{\mathbf{m}_{i-1}}^{\mathbf{m}_i}(t_i)\, A_{\mathbf{m}_{j-1}}^{\mathbf{m}_j}(t_j)\rangle.$$

Using (2.15*b*) and taking the IDA limit the second moment can be written in the form

$$\left.\begin{aligned} &\langle A_{\mathbf{k}}^{\mathbf{m}}(t_1)\, A_{\mathbf{k}'}^{\mathbf{m}'}(t_2)\rangle = -\delta_{(\mathbf{k}'-\mathbf{m})-(\mathbf{k}'-\mathbf{m}')} P_{\mathbf{k}-\mathbf{m}}(t_1 - t_2), \\ &P_{\mathbf{l}}(t) = h_{\mathbf{l}}^2(\mathbf{K} \pm \tfrac{1}{2}\mathbf{l}, \mathbf{K} \mp \tfrac{1}{2}\mathbf{l})\,[C_{\mathbf{l}}^*(t)\, e^{i\Delta_- t} + C_{\mathbf{l}}(t)\, e^{i\Delta_+ t}]\langle |c_{\mathbf{l}}|^2\rangle. \end{aligned}\right\} \tag{3.3}$$

† In general, ν_{P} may have added to it an imaginary term in this equation.

In this expression $\mathbf{k}$ and $\mathbf{m}$ are set to $\mathbf{K} \pm \frac{1}{2}\mathbf{l}$ where $\mathbf{K}$ is some *fixed* wavenumber representative of the set $(\mathbf{k}, \mathbf{m}, \mathbf{k}', \mathbf{m}')$. The frequency differences (2.15*c*) become

$$\Delta_{\pm} = \omega_{\mathbf{k}} - \omega_{\mathbf{k}\pm\mathbf{l}} \pm \omega_{\mathbf{l}}. \tag{3.4}$$

It is essential for the following that $P_{\mathbf{l}}$ vary only with $\mathbf{l}$, and therefore that the wavenumber $\mathbf{K}$ is treated as a constant. Using this property with (3.3), we rewrite (3.2) in the form

$$\gamma_{\mathrm{L}} = \sum_{\mathbf{m}_1 \ldots \mathbf{m}_{2n-1}} \sum_{\text{combinations}} \prod_{\text{pairs}} [-\delta_{(\mathbf{m}_{i-1}-\mathbf{m}_i)+(\mathbf{m}_{j-1}-\mathbf{m}_j)} P_{\mathbf{m}_{i-1}-\mathbf{m}_i}(t_i - t_j)], \tag{3.5}$$

where $\prod_{\text{pairs}}$ is the product over the n pairs (i,j) and the sum over combinations implies a sum over all distinct pairings of the indices.

Define a new set of wavenumbers

$$\mathbf{l}_i \equiv \mathbf{m}_{i-1} - \mathbf{m}_i \quad (i = 1, 2, \ldots, 2n)$$

so that (3.5) becomes

$$\gamma_{\mathrm{L}} = \sum_{\text{comb.}} \sum_{\mathbf{l}_1 \ldots \mathbf{l}_{2n}} \delta_{\mathbf{m}_0 - \mathbf{m}_{2n} - \sum_s \mathbf{l}_s} \prod_{\text{pairs}} [-\delta_{\mathbf{l}_i + \mathbf{l}_j} P_{\mathbf{l}_j}(t_i - t_j)].$$

The product of δ-functions implies that $\sum_s \mathbf{l}_s = 0$, so

$$\gamma_{\mathrm{L}} = \delta_{\mathbf{m}_0 - \mathbf{m}_{2n}} \sum_{\text{comb.}} \prod_{\text{pairs}} [-\sum_{\mathbf{l}} P_{\mathbf{l}}(t_i - t_j)]. \tag{3.6}$$

Notice that the Ps can be freely permuted in (3.6), since the matrix subscripts in the product have disappeared. Therefore the time-ordered product in (3.1) has no effect on the order of the Ps and (3.1) becomes

$$\begin{aligned} U_{\mathbf{k}}^{\mathbf{m}} &= \delta_{\mathbf{k}-\mathbf{m}} \sum_n \frac{1}{(2n)!} \sum_{\text{comb.}} \left[-\int_0 dt_1 \int_0^{t} dt_2 \, T \sum_{\mathbf{l}} P_{\mathbf{l}}(t_1 - t_2) \right]^n \\ &= \delta_{\mathbf{k}-\mathbf{m}} \exp\left[-\int_0^{t} dt' \, K_{\mathrm{L}}(t') \right]. \end{aligned} \tag{3.7}$$

Here the relaxation 'rate' K_{L} is defined as

$$K_{\mathrm{L}}(t') = \int_0^{t} dt'' \sum_{\mathbf{l}} P_{\mathbf{l}}(t' - t''). \tag{3.8}$$

These equations can be rewritten in the Langevin form by differentiation of (3.1) and using (3.7):

$$\frac{\partial}{\partial t} \langle b_{\mathbf{k}}(t) \rangle = -K_{\mathrm{L}}(t) \langle b_{\mathbf{k}}(t) \rangle. \tag{3.9}$$

The proper choice in K_{L} of the *fixed wavenumber* $\mathbf{K}$ is evidently $\mathbf{K} = \mathbf{k}$, the only available wavenumber vector. The associated uncertainty in the value of h_I is estimated from (2.18) to be less than 1 % for the allowed region in figure 1.

The Van Kampen (1974*a*, *b*) perturbation theory also leads to a Langevin equation of the form (3.9). The quantity K_{L} is expressed by Van Kampen formally as an infinite series of time-ordered cumulants. The leading term in this series is

$$K_{\mathrm{L}}(k, t) = -\int_0^{t} d\tau \sum_{\mathbf{m}} \langle A_{\mathbf{k}}^{\mathbf{m}}(t) \, A_{\mathbf{m}}^{\mathbf{k}}(t - \tau) \rangle. \tag{3.10}$$

This may be evaluated using (2.15*b*) and (2.19) as

$$K_{\mathrm{L}}(\mathbf{k}, t) = \pi \sum_{\mathbf{lm}} h(\mathbf{k}, \mathbf{m}) \, h(\mathbf{m}, \mathbf{k}) \, [D_{-}(t) \, \delta_{\mathbf{k}-\mathbf{m}-\mathbf{l}} + D_{+}(t) \, \delta_{\mathbf{k}-\mathbf{m}+\mathbf{l}}] \langle |c_{\mathbf{l}}|^2 \rangle, \tag{3.11}$$

where $D_\pm$ is defined by

$$D_\pm(t) \equiv \frac{1}{\pi}\int_0^t d\tau\, C_1(\pm\tau)\, e^{i\Delta_\pm \tau} \simeq \frac{1}{\pi}\int_0^t d\tau \exp(i\Delta_\pm \tau). \tag{3.12}$$

The last form follows, since we have agreed to set $\tau_c^{-1} = 0$ (equation (2.20)) and treat the large-scale field as linear.

If we neglect the contribution from h_N (2.16) here, the expressions (3.8) and (3.11) differ only by the assignment of the mean wavenumber **K** in (3.3). In the IDA limit (3.8) and (3.11) are identical. Therefore, in the allowed region of figure (1) the numerical distinction between these expressions is dominated by the contribution from h_N, which will be discussed in § 3.2.

The second non-vanishing term in the Van Kampen series is $O(A^4)$. The simplified form (2.18) for h has been used to provide an approximate evaluation of this term. The contribution from this is non-zero only because of the $O(l_z/k_z)^4$ terms and was found to be no more than 0·1 % in the allowed region of figure 1. That corrections from higher-order terms in the Van Kampen series are very small was anticipated from our comparison of (3.8) and (3.11).

The real part of K_L,

$$K_P(\mathbf{k}, t) \equiv \mathscr{R}(K_L), \tag{3.13}$$

determines the decay rate of the correlation function $\langle b_{\mathbf{k}}(t)\, b_{\mathbf{k}}(0)\rangle$, according to (3.9). As t becomes large, K_P approaches a constant limit, $K_P(\mathbf{k}, \infty)$. An approximate analytic form for K_P may be obtained by treating h as a fixed constant in (3.11):†

$$K_P(k, t) \simeq K_P(k, \infty)\,[1 + (\tau_a f)\sin(ft)\exp(-t/\tau_a) - \cos(ft)\exp(-t/\tau_a)], \tag{3.14}$$

$$\tau_a = (k_h B)/3\pi\omega_{\mathbf{k}}. \tag{3.15}$$

A generalized Langevin rate constant ν_P may be defined by the condition that

$$\int_0^{\nu_P^{-1}} K_P(\mathbf{k}, t)\, dt = 1. \tag{3.16}$$

Thus, ν_P^{-1} represents the first e-folding period for the decay of the autocorrelation of the $b_{\mathbf{k}}$.

In the limiting case that

$$\nu_P \tau_a \ll 1, \tag{3.17}$$

we have

$$\nu_P = K_P(\mathbf{k}, \infty). \tag{3.18}$$

The approximation (3.18) is that used by PMW and also gives the ν_P in the Hasselmann transport equation (1.1). We expect this *static* (or resonant-triad) approximation to be valid to the left and below the dashed curve in figure 1 (defining the boundary of the weak-interaction regime).

3.2. *Computation of the Langevin rate*

For the GM internal-wave model, it is an excellent approximation to set $\mathbf{m}_h = \mathbf{k}_h$ in h and $\Delta\pm$ in (3.11). If we also set $\omega_1 = f$ we may use (2.21) and (2.22) to obtain

$$K_P(k_z, \infty) = \frac{\pi}{(Bf)^2}\int dm_z\, \Phi(k_z - m_z)\, h(\mathbf{k}, \mathbf{m})\, h(\mathbf{m}, \mathbf{k})\,\{\delta(\omega_{\mathbf{k}} - \omega_{\mathbf{m}} - f) + \delta(\omega_{\mathbf{k}} - \omega_{\mathbf{m}} + f)\}, \tag{3.19}$$

† The numerical evaluation presented in § 3.2 shows that (3.14) is a satisfactory approximation for $K_P(\mathbf{k}, t)$.

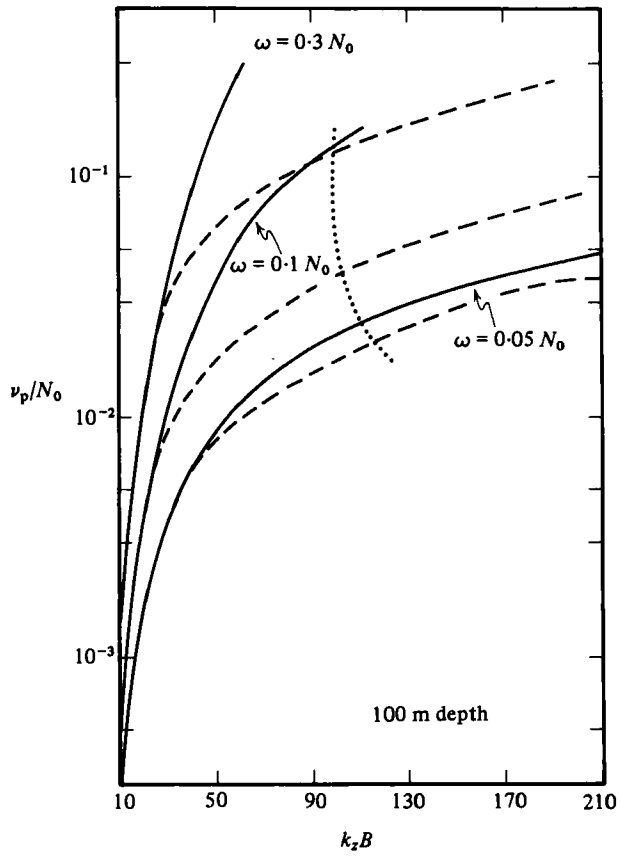

FIGURE 2. The solid curves represent the decorrelation constant $K_P(k_z, \infty)$ (3.19) displayed in units of N_0 at the depth of 100 m for several values of the frequency ω_k. The dashed curves represent the quantity ν_P/N_0 obtained from (3.16). The condition (3.20) is satisfied in the domain to the right of the dotted curve.

where it is understood that $\mathbf{m}_h = \mathbf{k}_h$. For specific calculations we shall use the values for N_0, f, and B specified in § 2.2.

Values of $K_P(k_z, \infty)/N_0$, obtained from (3.19), are shown as the solid curves in figures 2 and 3, corresponding to depths of 100 and 2000 m. Equation (3.19) was evaluated using both the full $h_I + h_N$ and the simplified h_I form of the coupling coefficients (2.16). The maximum contribution from h_N to the allowed region in figure 1 occurs along the boundary at $\omega/f = 5$. Since this corresponds to a correction of only 10 % at most, the simplified form with $h = h_I$ seems to be adequate in the *allowed region*. To a comparable degree of accuracy, we might also have used the form (2.17) for h_I.

Corrected values for ν_P using (3.16) are shown as the dashed curves in figure 2. In the strong-interaction regime the Langevin rate is much less than that predicted by the static, *resonant-triad* approximation represented by (3.19).

In figure 4 we show the Langevin rate ν_P as a function of ω and mode number j, where we have set $n(z) = 1$ and j is calculated as k_zB/π.† For $j \geqslant 10$ and $\omega/f = 5$,

† With the substitution $k_zB = \pi(j - \frac{1}{2})$, (3.19) agrees precisely with the corresponding expression (36) of PMW in the IDA.

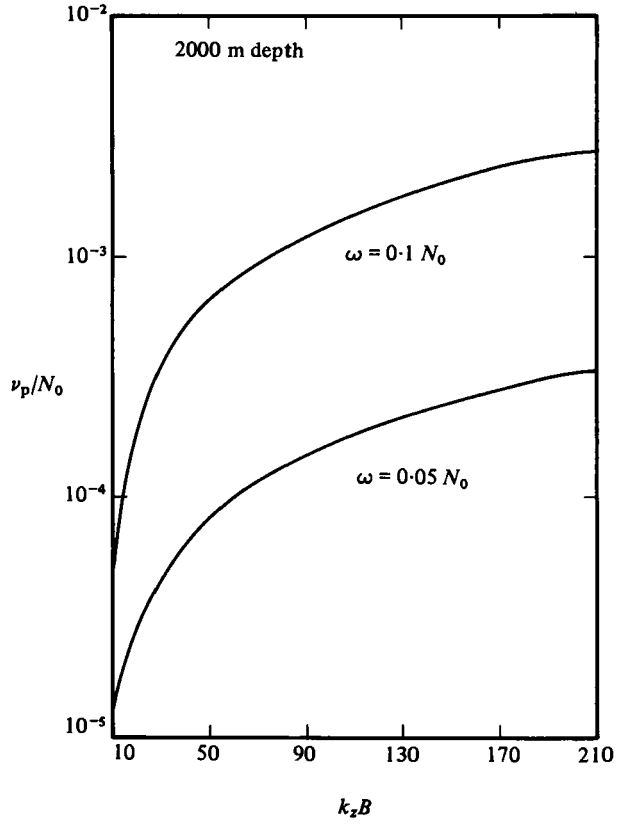

FIGURE 3. The constant $K_p(k_s, \infty)/N_0$, is shown for a depth of 2000 m.

we have used (3.16). The curves for $j = 1$, 3, and 5 for $\omega/f < 5$ are taken from figure 1 of PMW. The dashed curve represents the equation $\nu_p = \omega$. The striking modification of ν_p may be seen on comparing figure 4 with the corresponding figure 1 of PMW.

The domain

$$\omega_k/k_h < \langle U^2\rangle^{\frac{1}{2}}, \tag{3.20}$$

where $\langle U^2\rangle$ is given by (2.25), is bounded by the dotted curve in figure 2. It is interesting to note that the condition $\omega_k = k_h\langle U^2\rangle^{\frac{1}{2}}$ is met at $K_p(k_s, \infty) \simeq 0{\cdot}4\omega_k$.

4. Action transport

4.1. *The action-transport equation*

In this section we discuss the flow of action density in wavenumber and co-ordinate space by introducing the 'Wigner' distribution (Wigner 1932)

$$F(\mathbf{K}, \mathbf{r}) \propto \frac{1}{\Delta k_h^2 \Delta k_z} \sum_{\mathbf{p}} e^{i\mathbf{p}\cdot\mathbf{r}} \langle a^*_{\mathbf{K}-\frac{1}{2}\mathbf{p}} a_{\mathbf{K}+\frac{1}{2}\mathbf{p}}\rangle.$$

Using the action-amplitude variables of (2.12) and the assumption that the internal-wave field varies slowly in space on the scale of the wavelength $2\pi/K$, we obtain

$$F(\mathbf{K}, \mathbf{r}) \simeq \frac{1}{\Delta k_h^2 \Delta k_z} \sum_{\mathbf{p}} e^{i\mathbf{p}\cdot(\mathbf{r}-\mathbf{V}t)} \langle b^*_{\mathbf{K}-\frac{1}{2}\mathbf{p}} b_{\mathbf{K}+\frac{1}{2}\mathbf{p}}\rangle, \tag{4.1}$$

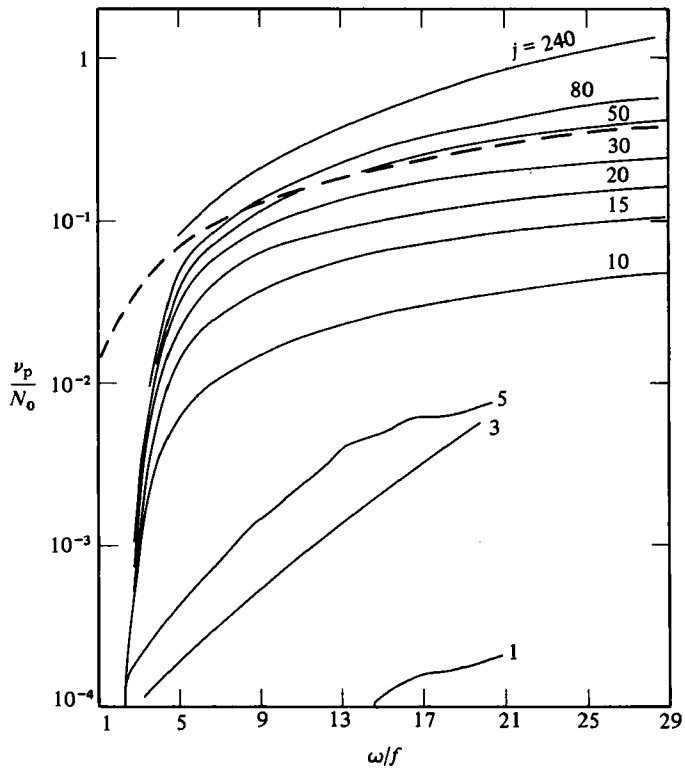

FIGURE 4. The Langevin rate ν_P is shown for various mode numbers j and frequencies ω. The dashed curve corresponds to $\omega = \nu_P$.

where the group velocity $\mathbf{V}(\mathbf{K}) \equiv \nabla_{\mathbf{K}}\omega_{\mathbf{K}}$. The normalization has been chosen so that the total action per unit volume is

$$F(\mathbf{r}) = \int d^3\mathbf{K}\, F(\mathbf{K}, \mathbf{r}),$$

and the total energy and momentum per unit volume are

$$E(\mathbf{r}) = \int d^3\mathbf{K}\, F(\mathbf{K}, \mathbf{r})\, \omega_{\mathbf{K}}, \quad \mathbf{M}(\mathbf{r}) = \int d^3\mathbf{K}\, F(\mathbf{K}, \mathbf{r})\, \mathbf{K}. \tag{4.2}$$

The derivation of a transport equation for (4.1) begins with the introduction of

$$Y(\mathbf{k}, \mathbf{m}, t) = b^*_{\mathbf{k}}(t)\, b_{\mathbf{m}}(t), \tag{4.3}$$

which, by (2.15), satisfies the equation

$$\dot{Y}(\mathbf{k}_1, \mathbf{m}_1, t) = \sum_{\mathbf{k}_2\mathbf{m}_2} A_{\mathbf{k}_1\mathbf{m}_1}{}^{\mathbf{k}_2\mathbf{m}_2}(t)\, Y(\mathbf{k}_2, \mathbf{m}_2, t). \tag{4.4}$$

Here $\mathbf{A}$ is given by

$$A_{\mathbf{k}_1\mathbf{m}_1}{}^{\mathbf{k}_2\mathbf{m}_2} \equiv \delta_{\mathbf{k}_1-\mathbf{k}_2} A_{\mathbf{m}_1}{}^{\mathbf{m}_2} + \delta_{\mathbf{m}_1-\mathbf{m}_2} A_{\mathbf{k}_1}{}^{\mathbf{k}_2 *}. \tag{4.5}$$

We wish to obtain a differential equation for the ensemble-averaged quantity $\langle Y(\mathbf{k}, \mathbf{m}, t)\rangle$. As a first step, we integrate formally (4.4):

$$\langle Y(\mathbf{k}_0, \mathbf{m}_0, t)\rangle = \sum_n \frac{1}{(2n)!} \int_0^t dt_1 \cdots \int_0^t dt_{2n} \sum_{\mathbf{k}_{2n}\mathbf{m}_{2n}} T\{\gamma_{\mathbf{B}\mathbf{k}_0\mathbf{m}_0}{}^{\mathbf{k}_{2n}\mathbf{m}_{2n}}(t_1, \ldots, t_{2n})\}\, Y(\mathbf{k}_{2n}, \mathbf{m}_{2n}, 0), \tag{4.6}$$

$$\gamma_{\mathbf{B}\mathbf{k}_0\mathbf{m}_0}{}^{\mathbf{k}_{2n}\mathbf{m}_{2n}}(t_1,\ldots,t_{2n}) \equiv \sum_{\mathbf{k}_1\ldots\mathbf{k}_{2n-1}} \sum_{\mathbf{m}_1\ldots\mathbf{m}_{2n-1}} \langle A_{\mathbf{k}_0\mathbf{m}_0}{}^{\mathbf{k}_1\mathbf{m}_1}(t_1)\, A_{\mathbf{k}_1\mathbf{m}_1}{}^{\mathbf{k}_2\mathbf{m}_2}(t_2)\ldots A_{\mathbf{k}_{2n-1}\mathbf{m}_{2n-1}}{}^{\mathbf{k}_{2n}\mathbf{m}_{2n}}(t_{2n})\rangle, \quad (4.7)$$

where the labels on the ts are chosen consistently with the time ordering implied in (4.6).

The moment (4.7) may be evaluated in terms of the second moments since **A** (4.5) is assumed Gaussian:

$$\langle A_{\mathbf{k}_1\mathbf{m}_1}{}^{\mathbf{q}_1\mathbf{p}_1}(t_1)\, A_{\mathbf{k}_2\mathbf{m}_2}{}^{\mathbf{q}_2\mathbf{p}_2}(t_2)\rangle = \{-\delta_{(\mathbf{k}_1-\mathbf{q}_1)+(\mathbf{k}_2-\mathbf{q}_2)}\,\delta_{(\mathbf{m}_1-\mathbf{p}_1)+(\mathbf{m}_2-\mathbf{p}_2)} + \delta_{(\mathbf{k}_1-\mathbf{q}_1)-(\mathbf{m}_2-\mathbf{p}_2)}\,\delta_{(\mathbf{m}_1-\mathbf{p}_1)-(\mathbf{k}_2-\mathbf{q}_2)}\}\, P_{(\mathbf{k}_1-\mathbf{q}_1),(\mathbf{m}_1-\mathbf{p}_1)}(t_1-t_2), \quad (4.8)$$

$$P_{\mathbf{l},\mathbf{p}}(\tau) \equiv \delta_{\mathbf{p}} P_{\mathbf{l}}^{*}(\tau) + \delta_{\mathbf{l}} P_{\mathbf{p}}(\tau).$$

The quantities $P_{\mathbf{l}}$ are defined by (3.3) and we are again assuming the IDA limit.

The moment (4.7) may now be expressed in a form analogous to (3.5):

$$\gamma_{\mathbf{B}} = \sum_{\text{comb. } \mathbf{k}_1\ldots\mathbf{k}_{2n-1}} \sum_{\mathbf{m}_1\ldots\mathbf{m}_{2n-1}} \prod_{\text{pairs}} \{-\delta_{(\mathbf{k}_{i-1}-\mathbf{k}_i)+(\mathbf{k}_{j-1}-\mathbf{k}_j)}\,\delta_{(\mathbf{m}_{i-1}-\mathbf{m}_i)+(\mathbf{m}_{j-1}-\mathbf{m}_j)} + \delta_{(\mathbf{k}_{i-1}-\mathbf{k}_i)-(\mathbf{m}_{j-1}-\mathbf{m}_j)}\,\delta_{(\mathbf{m}_{i-1}-\mathbf{m}_i)-(\mathbf{k}_{j-1}-\mathbf{k}_j)}\}\, P_{(\mathbf{k}_{i-1}-\mathbf{k}_i),(\mathbf{m}_{i-1}-\mathbf{m}_i)}(t_i-t_j). \quad (4.9)$$

Here as in § 3 $\sum_{\text{comb.}}$ implies a sum over all combinations of pairs of As.

Define a new set of summation variables

$$\mathbf{l}_i \equiv \mathbf{k}_{i-1}-\mathbf{k}_i, \quad \mathbf{p}_i \equiv \mathbf{m}_{i-1}-\mathbf{m}_i \quad (i=1,2,\ldots,2n); \quad (4.10)$$

and rewrite (4.9) as

$$\gamma_{\mathbf{B}} = \sum_{\text{comb. } \mathbf{l}_1\ldots\mathbf{l}_{2n}} \sum_{\mathbf{p}_1\ldots\mathbf{p}_{2n}} \delta_{\mathbf{k}_0-\mathbf{k}_{2n}-\sum_s \mathbf{l}_s}\,\delta_{\mathbf{m}_0-\mathbf{m}_{2n}-\sum_s \mathbf{p}_s} \times \prod_{\text{pairs}} [-\delta_{\mathbf{l}_i+\mathbf{l}_j}\delta_{\mathbf{p}_i+\mathbf{p}_j} + \delta_{\mathbf{l}_i-\mathbf{p}_j}\delta_{\mathbf{p}_i-\mathbf{l}_j}]\, P_{\mathbf{l}_i,\mathbf{p}_i}(t_i-t_j). \quad (4.11)$$

The δ-functions imply $\Sigma_s \mathbf{l}_s = \Sigma_s \mathbf{p}_s$, so we may set

$$\delta_{\mathbf{m}_0-\mathbf{m}_{2n}-\sum_s \mathbf{p}_s} = \delta_{(\mathbf{k}_0-\mathbf{k}_{2n})-(\mathbf{m}_0-\mathbf{m}_{2n})}$$

and remove this from the sums. The **p**-sums may now be done to give

$$\gamma_{\mathbf{B}} = \delta_{(\mathbf{k}_0-\mathbf{k}_{2n})-(\mathbf{m}_0-\mathbf{m}_{2n})} \sum_{\text{comb. } \mathbf{l}_1\ldots\mathbf{l}_{2n}} \delta_{\mathbf{k}_0-\mathbf{k}_{2n}-\sum_s \mathbf{l}_s} \prod_{\text{pairs}} \sum_{\mathbf{p}} [-\delta_{\mathbf{l}_i+\mathbf{l}_j} + \delta_{\mathbf{l}_j-\mathbf{p}}]\, P_{\mathbf{l}_i,\mathbf{p}}(t_i-t_j). \quad (4.12)$$

Next define another set of wavenumbers $\mathbf{k}_\alpha$ satisfying

$$\delta_{\mathbf{k}_0-\mathbf{k}_{2n}-\sum_s \mathbf{l}_s} = \sum_{\mathbf{k}_1\ldots\mathbf{k}_{n-1}} \prod_{\alpha=1}^{n} \delta_{\mathbf{k}_{\alpha-1}-\mathbf{k}_\alpha-(\mathbf{l}_{i\alpha}+\mathbf{l}_{j\alpha})}. \quad (4.13)$$

We have let the new variable $\mathbf{k}_n$ be equal to the old k_{2n}, and also designated the pairs $i-j$ by subscripts α. Substituting (4.13) into (4.12) and carrying out the **l**-sums gives

$$\gamma_{\mathbf{B}} = \delta_{(\mathbf{k}_0-\mathbf{k}_{2n})-(\mathbf{m}_0-\mathbf{m}_{2n})} \sum_{\text{comb. } \mathbf{k}_1\ldots\mathbf{k}_{n-1},} \prod_{\alpha=1}^{n} \sum_{\mathbf{l},\mathbf{p}} [-\delta_{\mathbf{k}_{\alpha-1}-\mathbf{k}_\alpha} + \delta_{\mathbf{k}_{\alpha-1}-\mathbf{k}_\alpha-(\mathbf{l}+\mathbf{p})}]\, P_{\mathbf{l},\mathbf{p}}(t_{i\alpha}-t_{j\alpha}). \quad (4.14)$$

Now expand the first δ-function in terms of a new set of variables $\mathbf{m}_\alpha$:

$$\delta_{(\mathbf{k}_0-\mathbf{k}_{2n})-(\mathbf{m}_0-\mathbf{m}_{2n})} = \sum_{\mathbf{m}_1\ldots\mathbf{m}_{n-1}} \prod_{i=1}^{n} \delta_{(\mathbf{k}_{i-1}-\mathbf{k}_i)-(\mathbf{m}_{i-1}-\mathbf{m}_i)}, \quad (4.15)$$

where the new variable $\mathbf{m}_n$ is equal to the old variable $\mathbf{m}_{2n}$. Substitution of the result into (4.6) yields

$$\langle Y(\mathbf{k}_0,\mathbf{m}_0,t)\rangle = \sum_{\mathbf{k}_1\ldots\mathbf{k}_n}\sum_{\mathbf{m}_1\ldots\mathbf{m}_n}\int_0^t dt_1\int_0^{t_1}dt_2\ldots\int_0^{t_{n-1}}dt_n \times K_{\mathbf{k}_0\mathbf{m}_0}{}^{\mathbf{k}_1\mathbf{m}_1}(t_1)\ldots K_{\mathbf{k}_{n-1}\mathbf{m}_{n-1}}{}^{\mathbf{k}_n\mathbf{m}_n}(t_n)\,Y(\mathbf{k}_n,\mathbf{m}_n,0). \tag{4.16}$$

Here we have defined a transport matrix

$$K_{\mathbf{km}}{}^{\mathbf{k'm'}}(\tau) = 2[\delta_{(\mathbf{k}-\mathbf{k'})-(\mathbf{m}-\mathbf{m'})}K_{\mathrm{F}}(\mathbf{k}-\mathbf{k}',\tau)-\delta_{\mathbf{k}-\mathbf{k'}}\delta_{\mathbf{m}-\mathbf{m'}}K_{\mathrm{P}}(\tau)], \tag{4.17a}$$

$$K_{\mathrm{P}}(t) \equiv \frac{1}{2}\int_0^t dt'\sum_{\mathbf{lp}}P_{\mathbf{l},\mathbf{p}}(t-t') = \int_0^t dt'\,\mathscr{R}\sum_{\mathbf{l}}P_{\mathbf{l}}(t-t'), \tag{4.17b}$$

$$K_{\mathrm{F}}(\mathbf{p},t) \equiv \frac{1}{2}\int_0^t dt'\sum_{\mathbf{l}}P_{\mathbf{l},(\mathbf{p}-\mathbf{l})}(t-t') = \int_0^t dt'\,\mathscr{R}P_{\mathbf{p}}(t-t'). \tag{4.17c}$$

Differentiation of (4.16) with respect to time yields the transport equation for Y:

$$\frac{\partial}{\partial t}\langle Y(\mathbf{k},\mathbf{m},t)\rangle = \sum_{\mathbf{k'm'}}K_{\mathbf{km}}{}^{\mathbf{k'm'}}(t)\langle Y(\mathbf{k}',\mathbf{m}',t)\rangle. \tag{4.18}$$

If we do not wish to take the IDA limit, we may again use the lowest-order expression obtained from Van Kampen's perturbation theory. This transport equation has the same form as (4.17) and (4.18) except that, as before, the full coupling coefficients are used. For the Van Kampen form we replace the term K_{P} in (4.17) by the real part of (3.11). The term K_{F} is replaced by

$$K_{\mathrm{F}}(\mathbf{k},\mathbf{k}',t) = \pi\sum_{\mathbf{l}}h^2(\mathbf{k},\mathbf{k}')\,\mathscr{R}[D_-(t)\,\delta_{\mathbf{k}-\mathbf{k}'-\mathbf{l}}+D_+(t)\,\delta_{\mathbf{k}-\mathbf{k}'+\mathbf{l}}]\langle|c_{\mathbf{l}}|^2\rangle. \tag{4.19}$$

Thus the transport equation (4.18) is exact to the extent that the IDA limit is valid and the perturbation theory can be used to provide corrections to the IDA. We shall indicate presently the importance of these corrections for the internal wave model.

The transport equation for the Wigner function (4.1) is obtained by writing

$$\mathbf{k} = \mathbf{K}-\tfrac{1}{2}\mathbf{p},\quad \mathbf{m} = \mathbf{K}+\tfrac{1}{2}\mathbf{p},\quad \mathbf{k}' = \mathbf{K}'-\tfrac{1}{2}\mathbf{p},\quad \mathbf{m}' = \mathbf{K}'+\tfrac{1}{2}\mathbf{p},$$

where use has been made of the δ-functions appearing in (4.17a). In an approximation consistent with the derivation of (4.1) we take $|\mathbf{p}| \ll |\mathbf{K}|, |\mathbf{K}'|$. Then (4.18) becomes

$$\frac{\partial}{\partial t}\langle Y(\mathbf{K}-\tfrac{1}{2}\mathbf{p},\mathbf{K}+\tfrac{1}{2}\mathbf{p})\rangle = 2\sum_{\mathbf{K}'}K_{\mathrm{F}}(\mathbf{K},\mathbf{K}')\langle Y(\mathbf{K}'-\tfrac{1}{2}\mathbf{p},\mathbf{K}'+\tfrac{1}{2}\mathbf{p})\rangle - 2K_{\mathrm{P}}(\mathbf{K})\langle Y(\mathbf{K}-\tfrac{1}{2}\mathbf{p},\mathbf{K}+\tfrac{1}{2}\mathbf{p})\rangle. \tag{4.20}$$

Here we have neglected the corrections that are linear in the small wavenumber $\mathbf{p}$. These terms represent spatial gradients of the Wigner function on the largest scale of inhomogeneities of the wave field.

Application of the Fourier transformation of (4.1) to (4.20) gives the transport equation

$$\left.\begin{aligned}&\left[\frac{\partial}{\partial t}+\mathbf{V}(\mathbf{K}).\nabla_{\mathbf{r}}\right]F(\mathbf{K},\mathbf{r},t)=S(\mathbf{K},\mathbf{r},t),\\&S(\mathbf{K},\mathbf{r},t)=2\int d^3\mathbf{K}'\,\mathbf{K}_{\mathrm{F}}(\mathbf{K},\mathbf{K}',t)\,F(\mathbf{K}',\mathbf{r},t)-2K_{\mathrm{P}}(\mathbf{K},t)\,F(\mathbf{K},\mathbf{r},t).\end{aligned}\right\}\tag{4.21}$$

Here $\mathbf{V}(\mathbf{K})$ is the group velocity corresponding to wavenumber $\mathbf{K}$.

Because the transport coefficients here are time dependent, $t = 0$ can play a special role in using (4.21). When negligible redistribution of the action occurs during the correlation time τ_{a}, the time-independent form may be used. We may, of course, sequentially re-derive (4.21) at time intervals longer than the correlation time τ_{a}.

We note that, since the transport coefficients of (4.21) do not depend on the fine-scale flow, we could average over realizations of the fine-scale flow as well as the large-scale flow.

In the IDA we would set $h = h_I$ (2.16) in these equations. The symmetry of h_I implies (see (4.17))

$$\sum_{\mathbf{K}'}K_{\mathrm{F}}(\mathbf{K},\mathbf{K}',t)=K_{\mathrm{P}}(\mathbf{K},t)\quad\text{(IDA)}.\tag{4.22}$$

In this case it is clear from (4.21) that the total action is conserved by the wave scattering.

4.2. *Computation of internal-wave transport*

For our present applications we shall ignore the relatively slow transport in horizontal-wavenumber space. The inequalities (2.1) then imply that the horizontal components of $\mathbf{K}$ and $\mathbf{K}'$ may be set equal to some constant, say K_{h}, in (4.21). If we assume that F depends only on depth and vertical wavenumber (since the dependence on K_{h} can be suppressed) then (4.21) takes the form

$$\left.\begin{aligned}&\left[\frac{\partial}{\partial t}+\dot{z}\frac{\partial}{\partial z}+\dot{k}_z\frac{\partial}{\partial k_z}\right]F(k_z,z,t)=S(k_z,z,t),\\&S(k_z,z,t)=2\int dk_z'K_{\mathrm{F}}(k_z,k_z',t)\,F(k_z',z,t)-2K_{\mathrm{P}}(k_z,t)\,F(k_z,z,t),\end{aligned}\right\}\tag{4.23}$$

where the scattering rates are given by

$$\begin{aligned}K_{\mathrm{F}}(k_z,k_z',t)&\equiv\int d^2k_{\mathrm{h}}K_{\mathrm{F}}(\mathbf{k},\mathbf{k}',t)\\&=\frac{\pi}{(Bf)^2}\int dl_z\,\Phi(k_z-k_z')\,h^2(k_z,k_z')\,\mathscr{R}[D_-(t)\,\delta_{k_z-k_z'-l_z}+D_+(t)\,\delta_{k_z-k_z'+l_z}],\\K_{\mathrm{P}}(k_z,t)&=\frac{\pi}{(Bf)^2}\int dl_z\int dk_z'\,\Phi(k_z-k_z')\,h(k_z,k_z')\,h(k_z',k_z)\,\mathscr{R}[\ldots].\end{aligned}\tag{4.24}$$

Here $D_\pm$ is given by (3.12) and the brackets enclose the same expression for each rate. In the *static*, or *resonant-triad* approximation, we have

$$\mathscr{R}D_\pm=\delta(\omega_{\mathbf{k}}-\omega_{\mathbf{k}'}\pm f),$$

where we have again set $\omega_{\mathbf{l}}=f$.

We have introduced in the left-hand side of (4.23) an additional convective term

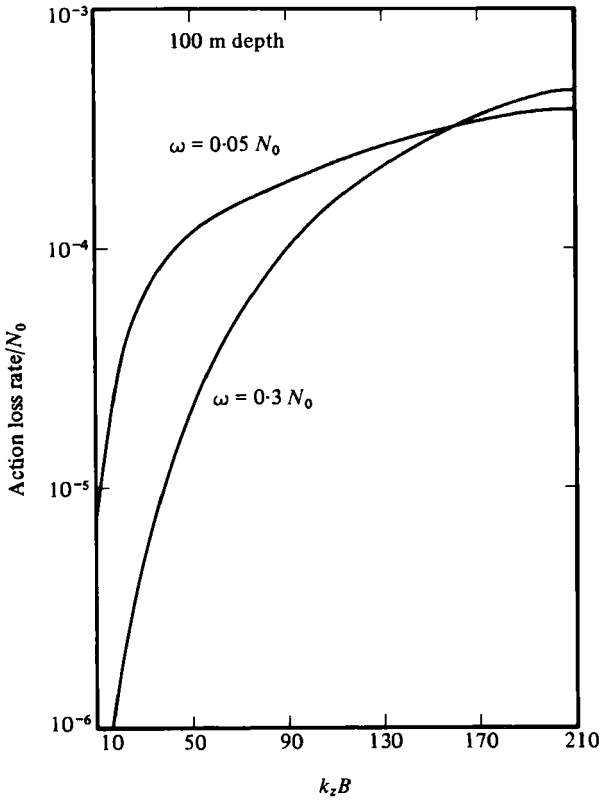

FIGURE 5. The net rate of action loss due to interaction with the large-scale flow (4.29).

to take account of the change of Väisälä frequency $N(z)$ with depth. A formal derivation of this term by the method of Watson & West (1975) gives the expression

$$\dot{k}_z = V_z(k_z)\, k_z \frac{d \ln N}{dz}. \tag{4.25}$$

This is just the WKB relation between N and the vertical component of wavenumber.

For the applications described in this section we shall make the resonant-triad approximation in (4.23). The k_z' integration in (4.24) may then be done, yielding

$$S(k_z, z, t) = \sum_{\sigma=\pm} K(k_z, k_z^\sigma) \left[\frac{h(k_z, k_z^\sigma)}{h(k_z^\sigma, k_z)} F(k_z^\sigma, z, t) - F(k_z, z, t) \right]. \tag{4.26}$$

Here $k_z^\pm$ is defined by the resonance condition

$$\omega_{k_z^\pm} = \omega_{k_z} \pm f, \tag{4.27}$$

$$K(k_z, k_z^\sigma) = \frac{2\pi}{(Bf)^2} \Phi(k_z - k_z^\sigma) \frac{h^2(k_z, k_z^\sigma)}{V_z(k_z^\sigma)}, \tag{4.28}$$

where the group velocity in K arises from the integration.

We can obtain an estimate of the corrections to the IDA by setting $F = F_0$, a

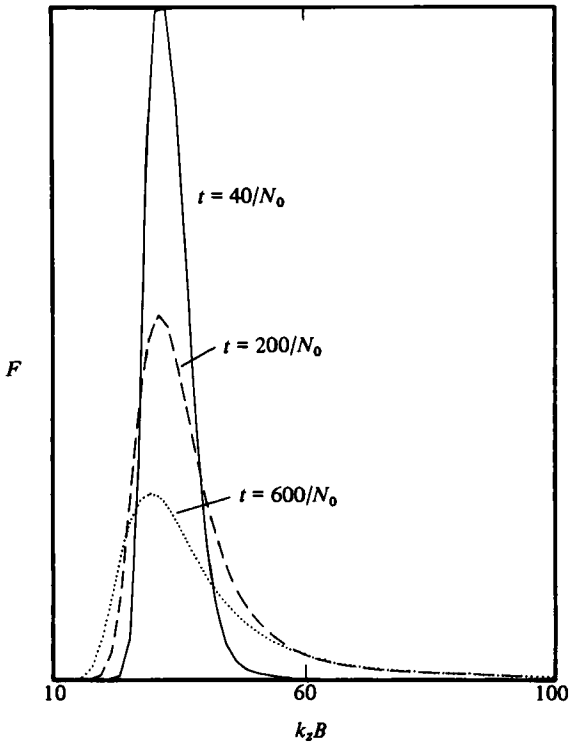

FIGURE 6. The transport of action from (4.32). The horizontal wavelength is 1000 m. The three curves are for times $tN_0 = 40$, 200 and 600, as indicated.

constant, in (4.26). The total action is then increasing owing to the interaction with the large-scale flow at the rate

$$\frac{1}{F_0}\frac{dF}{dt} = \sum_{\sigma=\pm} K(k_z, k_z^\sigma)\left[\frac{h(k_z, k_z^\sigma)}{h(k_z^\sigma, k_z)} - 1\right], \tag{4.29}$$

which of course vanishes in the IDA. This quantity is shown in figure 5 for $\omega = 0{\cdot}3N_0$ and $0{\cdot}05N_0$. Reference to figure 2 indicates that (4.29) is about two orders of magnitude smaller than K_P and so the corrections to the IDA are again very small.

For our subsequent discussion we shall accept the IDA as valid and set $h = h_I$ in (4.26) and (4.28) so that

$$S(k_z, z, t) = \sum_{\sigma=\pm} K(k_z, k_z^\sigma)\,[F(k_z^\sigma, z, t) - F(k_z, z, t)]. \tag{4.30}$$

The rates of change of energy and momentum are obtained from (4.2):

$$\left.\begin{aligned}\left.\frac{dM_z}{dt}\right|_{sc} &= -\int dk_z\, dk_z'\, K_F(k_z, k_z')\,[F(k_z, z, t) - F(k_z', z, t)]\,(k_z - k_z'),\\ \left.\frac{dE}{dt}\right|_{sc} &= -\int dk_z\, dk_z'\, K_F(k_z, k_z')\,[F(k_z, z, t) - F(k_z', z, t)]\,(\omega_{k_z} - \omega_{k_z'}).\end{aligned}\right\} \tag{4.31}$$

Thus, for example, a domain in which F decreases with increasing k_z contributes an increase in momentum and a decrease in energy (since ω decreases with increasing k_z) to the fine-scale flow. The transfer is to or from the large-scale flow, as the case may be.

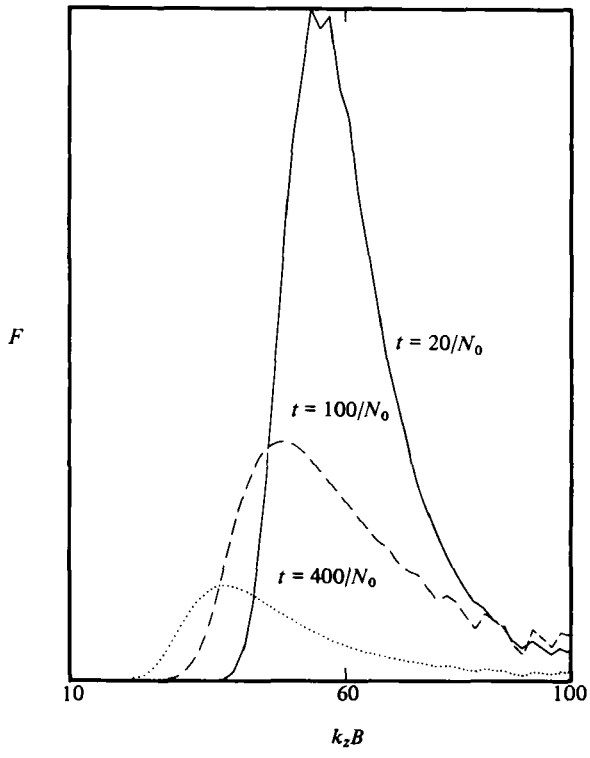

FIGURE 7. The computation of figure 6 is repeated for a modified initial condition. The three curves are at $tN_0 = 20$, 100 and 200.

When there is no z-dependence, (4.23) becomes

$$\frac{\partial}{\partial t}F(k_z, t) = S(k_z, t), \tag{4.32}$$

and is easily integrated numerically. As an example we choose an equally spaced grid in k_z between the limits $10 \leqslant k_zB \leqslant 100$. A reflecting barrier is placed at $k_zB = 10$ and an absorbing barrier at $k_zB = 100$. A computation is presented in figure 6 with an initial condition

$$F(k_z, 0) = \begin{cases} 1 & (26 < k_zB < 32), \\ 0 & (\text{otherwise}). \end{cases}$$

Because the rate constant K increases significantly with k_z, the transport is predominantly to higher wavenumbers with action flowing out of the system at $k_zB = 100$ owing to the absorbing barrier.

Figure 7 displays the transport of action given the initial condition

$$F(k_z, 0) = \begin{cases} 1 & (46 < k_zB < 52) \\ 0 & (\text{otherwise}). \end{cases}$$

Because K increases with k_z, the transport is more rapid than in figure 6. The jagged appearance of portions of the curves is due to the finite size of the steps $|k_z - k_z^\sigma|$.

We illustrate the loss of energy from the fine-scale field by choosing an initial

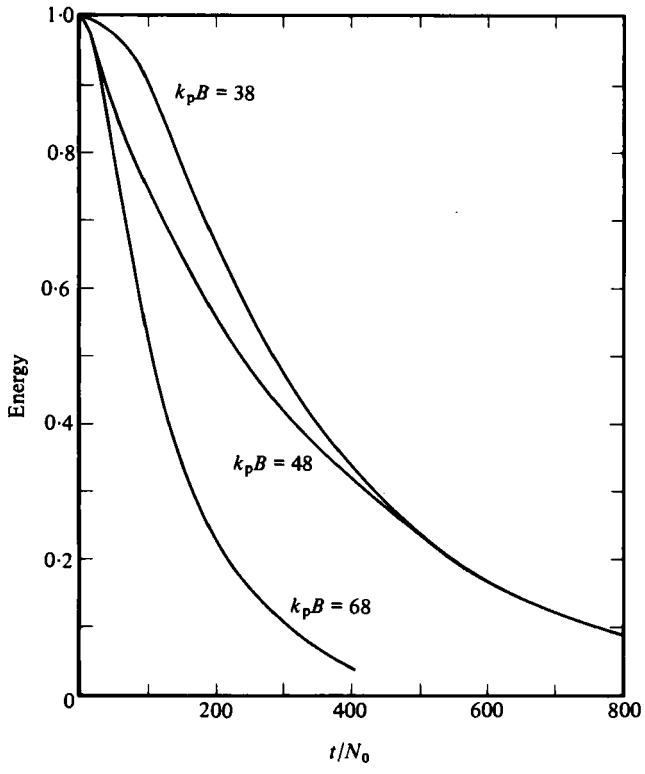

FIGURE 8. Decay of energy in the fine-scale flow from (4.31) in the resonant-interaction limit. At $t = 0$ the excitation is localized near the wavenumber k_p as indicated on the curves. The horizontal wavenumber is $12/B$.

distribution concentrated near a vertical wavenumber k_p. The absorbing barrier is placed at $k = k_p + 80/B$. The energy (4.2), normalized to unity at $t = 0$, is evaluated using (4.32) and displayed in figure 8 for several values of k_p. The principal energy loss is to the absorbing barrier. Because the rate constant K in (4.30) increases with k_z, energy absorption is insensitive to the precise location of the barrier.

We introduce an inverse Richardson number by

$$R^{-1} \equiv \frac{1}{N^2}\left\langle \left(\frac{\partial \mathbf{u}}{\partial z}\right)^2 \right\rangle,$$

where $\mathbf{u}$ is the horizontal component of the fine-scale velocity field. In figure 9, the time dependence of R^{-1} for the initial conditions of figures 6 and 7 is displayed. We have normalized R^{-1} to unity at $t = 0$.

When the Väisälä frequency depends on depth, the k_z term in (4.23) may be important. Use of the Garrett–Munk exponential profile, (2.24), in (4.25) yields

$$\dot{k}_z = \frac{V_z(k_z)}{B} k_z = \frac{\dot{z}}{B} k_z,$$

which may be integrated to obtain

$$k_z e^{-z/B} = k_s, \tag{4.33}$$

where k_s is constant in time and represents the effective surface vertical wavenumber.

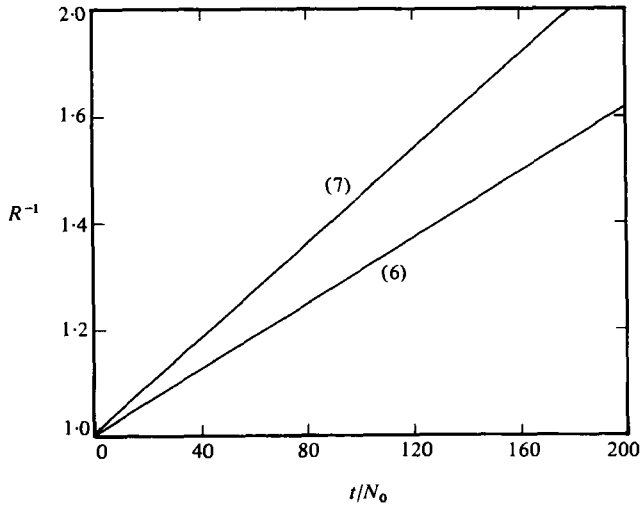

FIGURE 9. The variation of inverse Richardson number with time. The curves labelled (6) and (7) refer to the cases shown in figures 6 and 7, respectively.

The transport equation may be partially integrated by defining a new dependent variable

$$y = \int_{-\infty}^{z} \frac{dz}{\dot{z}} - t = \frac{B}{V_z(k_z)} - t. \tag{4.34}$$

In terms of k_s and y the transport equation (4.23) becomes

$$\left.\begin{aligned} W(k_s, y, t) &= F(k_z(y,t), z(k_s, y, t), t), \\ \frac{\partial}{\partial t} W(k_s, y, t) &= S(k_s, y, t). \end{aligned}\right\} \tag{4.35}$$

Once W is known, F may be obtained using (4.33) and (4.34).

In our computations the function $F(k_z, z, t = 0)$ is evaluated on a rectangular grid in (k_s, n)-space, where $n \equiv e^{z/B}$. As time increases k_s is constant, but n depends on time as implied by (4.33) and (4.34):

$$\frac{dn}{dt} = \frac{dn}{dz} V_z(k_z) = -\frac{\omega_k^2 - f^2}{\omega_k k_s B}.$$

Here the dispersion relation (2.11) has been used. For $\omega_k \gg f$ this becomes

$$\frac{dn}{dt} \simeq -N_0 \frac{k_h}{k_s^2 B},$$

so that convection is relatively more important for the small vertical wavenumbers.

For these computations absorbing boundary conditions have been chosen. A wave reaching the top ($n = 1$) or the bottom ($n = 0$) is absorbed.

In figure 10 we display a computation for $k_h B = 5$. The initial condition is a Gaussian bump centred at $k_s B = 83$ and $n(z) = 0{\cdot}44$. The sign of the wavenumber is chosen negative so that the convection is upward. The group velocity for $k_s B < 30$ is so large that the action is rapidly convected to the surface and lost from the computation.

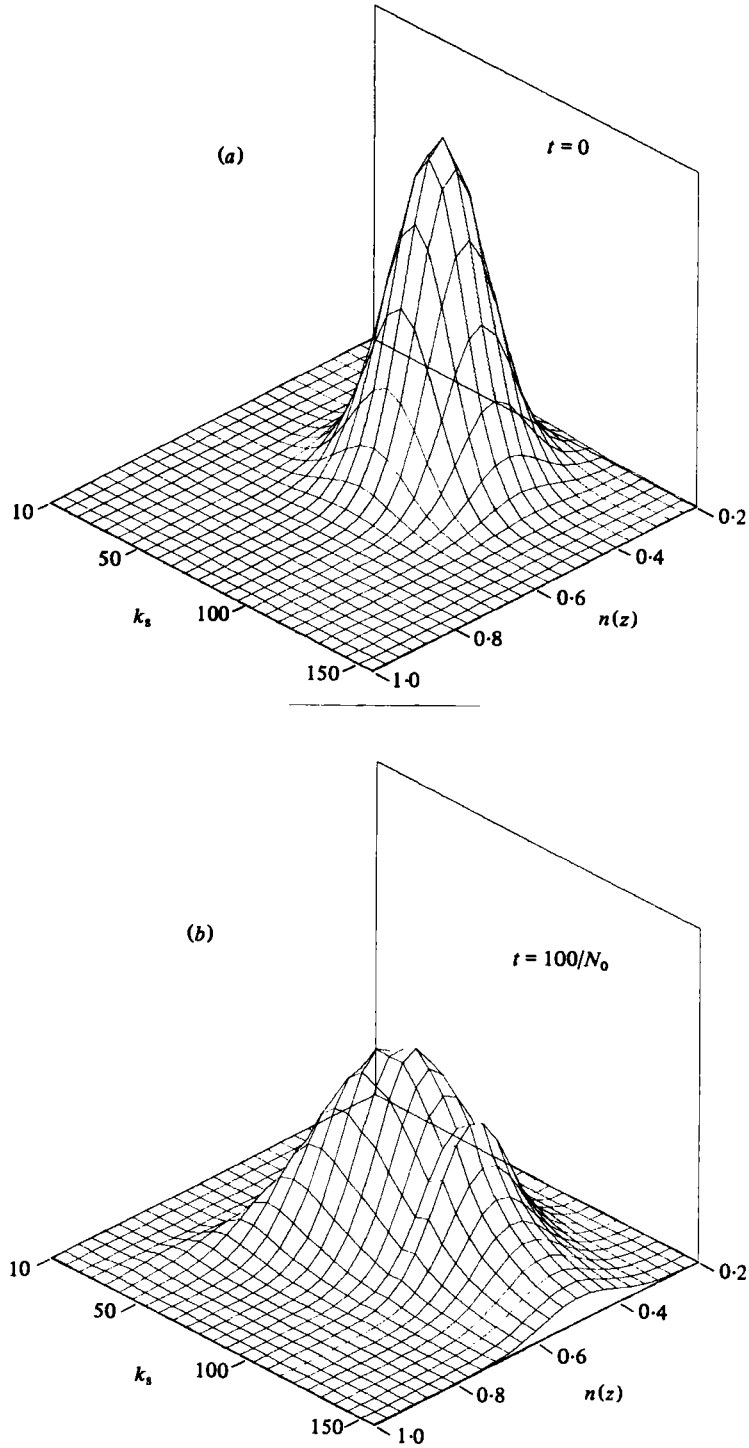

FIGURE 10 (*a*, *b*). Legend on p. 338.

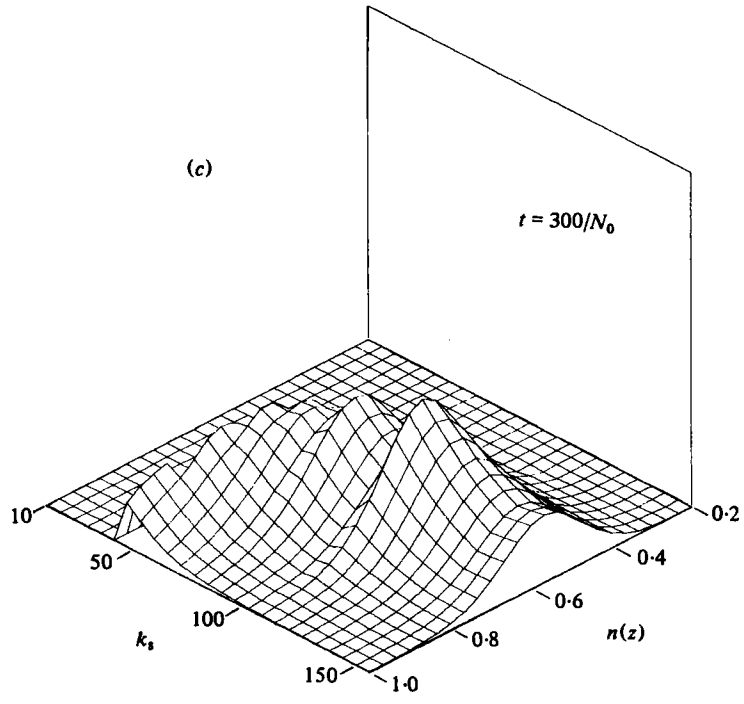

FIGURE 10. Integration of the Wigner-function transport equation (4.35) with $K_h B = 5$. The initial condition is a Gaussian bump with positive group velocity. (*a*) presents the initial condition, (*b*) is for $tN_0 = 100$, and (*c*) is for $tN_0 = 300$.

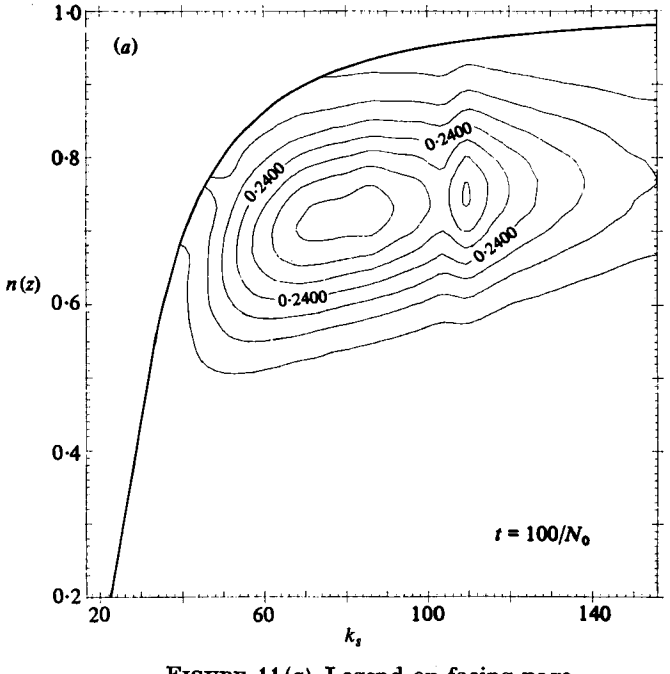

FIGURE 11 (*a*). Legend on facing page.

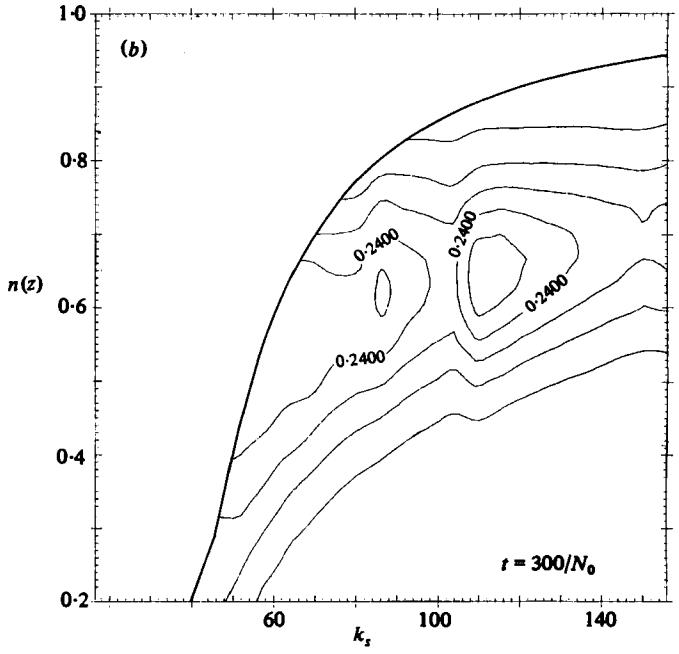

FIGURE 11. Contour plots of the Wigner function for an initial condition near the surface. The initial condition is similar to that in figure 10 except that the bump is centred at $n = 0{\cdot}8$. (*a*) is at $tN_0 = 100$, and (*b*) is at $tN_0 = 300$.

For greater wavenumbers, scattering dominates and the bump spreads relatively more rapidly in the wavenumber direction than in the spatial direction. As in figure 7 the jagged portions of the curves are due to the discrete steps from the resonance conditions. Total action is conserved by the algorithm to within 1 % for $tN_0 \leqslant 400$.

Figure 11 is a contour plot of a similar computation. Here we choose an initial Gaussian bump centred at $k_s B = 83$ and $n(z) = 0{\cdot}8$. The sign of wavenumber for this case is positive. The scattering is more rapid for this case since by (2.23) the magnitude of S in (4.35) is proportional to $n(z)$. In these figures the thick lines indicate the curve which begins at $t = 0$ as the ocean surface ($n = 1$). Action could only flow into the region above this boundary by reflection of $k_s < 0$ waves at the ocean surface.

5. The bispectrum

The bispectrum for the fine-scale flow may be obtained from the quantities

$$\langle b^*_{\mathbf{k}_1} b_{\mathbf{k}_2} b_{\mathbf{k}_3} \rangle. \tag{5.1}$$

If we assume that $\mathbf{k}_1$, $\mathbf{k}_2$ and $\mathbf{k}_3$ are all nearly equal to some constant $\mathbf{K}$, and furthermore that the expression (5.1) varies slowly when the ks vary over the range l_h, l_{iv}, then the Van Kampen perturbation theory gives

$$\frac{\partial}{\partial t} \langle b^*_{\mathbf{k}_1} b_{\mathbf{k}_2} b_{\mathbf{k}_3} \rangle = -K_P(\mathbf{K}, t) \langle b^*_{\mathbf{k}_1} b_{\mathbf{k}_2} b_{\mathbf{k}_3} \rangle. \tag{5.2}$$

Here we have assumed that the imaginary part of K_L vanishes.

6. Conclusions

The calculations reported by PMW used discrete vertical eigenfunctions to describe the linear internal-wave field. These were evaluated in the WKB approximation using the GM scaling (2.24). In the present paper we have followed Olbers and MB in using a three-dimensional Fourier representation and a locally constant Väisälä frequency. The distinction between these descriptions is not significant for our present work. In fact, if we set $k_z B = \pi(j - \frac{1}{4})$ and $n(z) = 1$ in (2.23), our expression (3.19) agrees precisely with the corresponding expression (36) of PMW when the IDA limit is taken.

The Langevin rate ν_P was seen in PMW to be a fundamental quantity in the theory of internal-wave transport processes. It provides the decay rate of the correlation function of the Fourier amplitudes, it provides the relaxation rates for McComas' (1977) 'bump experiments', and it was used by PMW to derive the full Hasselmann transport equation. We have given a prescription for calculating ν_P in the 'allowed region' of figure 1. This is the region in which the induced-diffusion mechanism is dominant. Corrections to the IDA appear to contribute at most about 10 % in this region. It is also the region for which the GM spectrum represents, in an approximation, an 'equilibrium solution' to the Hasselmann transport equation (the quantitative form of this statement is seen from figure 4 of PMW).

The transport equation (4.21) is also expected to be valid in the allowed region of figure 1. In the static, resonant-triad limit when $t \gg \tau_a$, this is equivalent to the IDA limit of the Hasselmann equation used by MB and by Olbers. The condition for use of the static limit in (4.21) must be determined for specific applications, since this depends on the initial form of F. If this does not differ significantly from the GM form and does not have sharp 'bumps', the static limit appears to be valid in the allowed region of figure 1. For a spectrum not close to 'equilibrium', the transport rates deduced from (4.21) are expected to be substantially less than would be obtained from the Hasselmann equation for the induced-diffusion domain.

The right-hand boundary in figure 1 corresponds to the limit at which Munk (1981) has anticipated that the internal-wave spectrum rolls off owing to instabilities. It also corresponds to the roll-off of temperature gradient spectra observed by Gregg (1977). A flow of internal wave energy across the lower and right-hand boundaries is predicted by the wave–wave transport theory.

The regions below and to the left of the allowed region do not correspond to 'equilibrium domains' for the GM spectrum, as calculated by MB and PMW. According to these calculations, energy flows out of the domain of $j < 10$ and into the domain $\omega < 5f$ (see, e.g., figure 8 of McComas 1977). The identification of the sources and sinks of energy in these non-equilibrium regions will presumably require consideration of other than just internal-wave–internal-wave interactions.

This research was partially supported by the Office of Naval Research under contracts N00014-78-C-0050 and N00014-79-C-0537. The authors would like to thank Dr Walter Munk for helpful suggestions concerning this work.

REFERENCES

BOOKER, J. R. & BRETHERTON, F. P. 1967 *J. Fluid Mech.* **27**, 513.

BRETHERTON, F. P. 1966 *Quart. J. R. Met. Soc.* **92**, 466.

COX, C. S. & JOHNSON, C. L. 1979 Inter-relations of microprocesses, internal waves, and large scale ocean features (unpublished manuscript).

DAVIDSON, R. C. 1972 *Methods in Nonlinear Plasma Theory*. Academic.

GARRETT, C. J. R. & MUNK, W. H. 1979 *Ann. Rev. Fluid Mech.* **11**, 339.

GREGG, M. C. 1977 *J. Phys. Oceanog.* **7**, 33.

HASSELMANN, K. 1966 *Rev. Geophys. Space Phys.* **4**, 1.

HASSELMANN, K. 1967 *Proc. R. Soc. Lond.* A **299**, 77.

HOLLOWAY, G. 1979 *Geophys. Astrophys. Fluid Dyn.* **11**, 271.

HOLLOWAY, G. 1980 *J. Phys. Oceanog.* **10**, 906.

HOLLOWAY, G. & HENDERSHOTT, M. C. 1977 *J. Fluid Mech.* **82**, 747.

MCCOMAS, C. H. 1977 *J. Phys. Ocean* **7**, 836.

MCCOMAS, C. H. & BRETHERTON, F. P. 1977 *J. Geophys. Res.* **82**, 1397.

MEISS, J. D., POMPHREY, N. & WATSON, K. M. 1979 *Proc. Nat. Acad. Sci. U.S.A.* **76**, 2109.

MÜLLER, P. 1976 *J. Fluid Mech.* **77**, 789.

MUNK, W. H. 1981 In *Evolution of Physical Oceanography* (ed. B. A. Warren & C. Wunsch), p. 264. MIT Press.

OLBERS, D. J. 1976 *J. Fluid Mech.* **74**, 375.

PHILLIPS, O. M. 1977 *The Dynamics of the Upper Ocean*, 2nd edn. Cambridge University Press.

PINKEL, R. 1975 *J. Geophys. Res.* **80**, 3892.

POMPHREY, N. 1981 In *Nonlinear Properties of Internal Waves* (ed. B. J. West), p. 103. American Institute of Physics.

POMPHREY, N., MEISS, J. D. & WATSON, M. K. 1980 *J. Geophys. Res.* **85**, 1085.

VAN KAMPEN, N. G. 1974*a* *Physica* **74**, 215.

VAN KAMPEN, N. G. 1974*b* *Physica* **74**, 239.

WATSON, K. M. 1981 In *Nonlinear Properties of Internal Waves* (ed. B. J. West), p. 193. American Institute of Physics.

WATSON, K. M. & WEST, B. J. 1975 *J. Fluid Mech.* **70**, 815.

WIGNER, E. P. 1932 *Phys. Rev.* **40**, 749.

YAU, P. 1981 Ph.D. thesis, Spectral transfer of the nonlinear internal wave field of the Upper Ocean. University of California, Berkeley.